Proceedings of the 21st ICSMGE, Vienna, Austria, 14 – 19 June 2026. Pistrol, Adam & Schweiger (eds.)
Published by: ÖGG, Austrian Society for Geomechanics, Salzburg, Austria, ISBN 978-3-9503898-4-5
https://doi.org/10.53243/ICSMGE2026-894

Experimental Assessment of the Stability of Masonry Retaining Walls Under Heavy Rainfall Using Reduced-Scale Models

Hicham Cherifi, Anne-Sophie Colas
Univ Gustave Eiffel, Univ Lyon, GERS-RRO, F-69675 Lyon, France, hicham.cherifi@univ-eiffel.fr

Benjamin Terrade
Univ Gustave Eiffel, MAST-EMGCU, F-77454 Marne-la-Vallée, France

Denis Garnier
Laboratoire Navier (UMR 8205), ENPC, Univ Gustave Eiffel, CNRS, 77455 Marne-la-Vallée, France

ABSTRACT: Masonry retaining walls are widespread roadside structures in Europe and represent about 60% of the French national inventory (Cerema, 2020). Although known for their durability, their long-term performance depends on adequate maintenance, particularly as climate change increases the frequency and intensity of extreme rainfall. Such events generate strong hydraulic pressure gradients that may destabilize these walls. This study investigates failure mechanisms induced by hydraulic loading through reduced-scale laboratory experiments. Masonry walls built with small bricks (35.0 mm × 18.5 mm × 11.5 mm) retained a saturated Hostun HN31 sand embankment and were subjected to simulated heavy rainfall. High-speed cameras, camcorders, and piezometers recorded deformation, displacement, and failure patterns in real time. The results were interpreted using a yield design framework and will support forthcoming numerical modeling with discrete element (3DEC ITASCA) and finite element approaches (DISROC). This combined methodology enabled the identification of failure modes, load–displacement responses, and comparison between experiments and theoretical predictions. The study ultimately contributes to improved predictive tools for assessing the safety of masonry retaining walls under extreme hydraulic conditions.

KEYWORDS: Masonry Walls, Retaining Structures, Hydraulic Load, Stability, yield design, Climate Impact.

1 INTRODUCTION

Masonry retaining walls represent a widespread category of gravity walls across Europe, especially in countries such as France and the United Kingdom. Their proliferation dates back to the 19th and early 20th centuries, paralleling the infrastructural expansion brought about by the Industrial Revolution. These structures display a broad range of characteristics, influenced by the nature of the construction materials, the geometry of the walls, the assembly techniques, and the types of joints employed. In France, masonry walls represent about 60% of the 6,000 retaining structures along national roads (Cerema, 2020) and nearly 90% of the 100,000 retaining structures along departmental roads, where their maintenance and long-term conservation remain complex and costly challenges.

Renowned for their robustness and ability to integrate well with their surroundings, these walls are nonetheless increasingly exposed to the adverse consequences of climate change (Kandalai et al., 2023; Phoon, 2023). Many were not conceived to endure today's extreme climatic phenomena. The intensification and rising frequency of intense or torrential rainfall events, especially in Mediterranean regions where such occurrences were previously rare, now demand that these be treated as accidental actions in design practices. This evolution necessitates a rethinking of design criteria and calls for the adaptation of existing technical standards and recommendations to incorporate climate-related risks (IPCC, 2022; PNACC, 2024). Moreover, enriching the scientific and technical understanding of masonry retaining walls is vital. A number of studies—such as those by Colas (2008), Le (2013), and Terrade (2018)—have employed analyses grounded in yield design theory to assess structural performance under loads such as self-weight, lateral earth pressure, and hydrostatic effects. Despite methodological differences, these works collectively rely on analytical tools, numerical optimization, and experimental validation, offering a rich and multidimensional evaluation framework.

Beyond static considerations, the dynamic and seismic behavior of masonry structures has also garnered attention. For instance, Savalle (2019) analyzed the seismic response of masonry retaining walls using a combination of Discrete Element Method (DEM) simulations and physical tests. These efforts underline the inherent complexity of modeling masonry. As a composite assembly of blocks and joints, masonry can be represented at different scales: as a homogenized continuum at the macroscopic level, as a simplified arrangement of units and joints at the mesoscopic level, or as a detailed configuration at the microscopic scale. According to Sarhosis et al. (2016), the most representative modeling strategy involves explicitly distinguishing between blocks and joints, with the DEM proving especially effective in this regard. While it offers comprehensive insights (e.g., stress, strain, displacements, internal pressures), the method requires a substantial number of parameters to define material behavior—parameters that are often difficult to determine—and comes with significant computational demands, particularly for hydro-mechanical coupled analyses.

In this context, the present experimental work is part of a broader research effort aimed at developing an analytical tool based on yield design theory to assess the stability of masonry retaining walls subjected to flow-induced forces generated by extreme hydraulic events. This analytical approach is supported by experimental validation through a series of tests conducted on reduced-scale physical models.

2 PROBLEM STATEMENT

The objective of this study is to determine the critical hydraulic height Hw that induces failure of the retaining wall, and to identify the realistic failure mechanisms involved. The applied hydraulic loading is characterized by its sudden and instantaneous nature, making it difficult to reproduce in full-scale structures. Consequently, identifying the relevant failure mechanisms constitutes a first major challenge. Current understanding is primarily based on normative documents and

research conducted since 2004 on this type of dry-jointed masonry wall, which has broadly highlighted three dominant failure modes: sliding, overturning, and a mixed mode combining aspects of both. The occurrence of a specific mode depends on the geometry of the system and the mechanical properties of the soil, the wall, and their interface.

In this study, the base of the wall is assumed to be fixed, in order to eliminate the influence of erosion or sliding at the base. This assumption is supported by several discrete element method (DEM) simulations coupled with hydro-mechanical modeling, applied to various geometries (Fig.1), which confirm the relevance of the failure mechanisms considered. As a result, the analytical developments presented are restricted to these three failure modes. Further analysis was conducted to evaluate the effect of joint opening not only on the geometry of the problem but more importantly on the stress distribution within the joints. This was achieved using an enriched finite element method (FEM-X) incorporating joint elements, implemented in a rock mechanics-oriented code (Disroc). The comparison between models with closed joints and those allowing for joint opening revealed minimal differences. However, a major limitation of these sensitivity analyses lies in the scarcity of reliable mechanical parameters for the masonry interface. For this purpose, the mechanical data from Savalle (2019) were used.

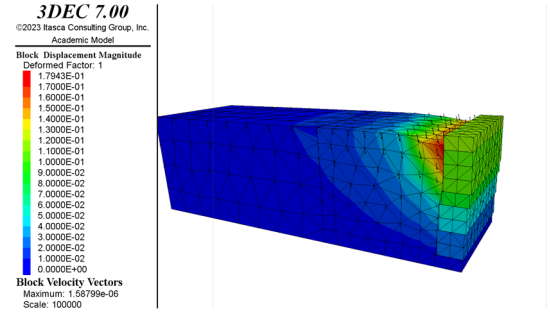

Figure 1: Example of a sliding mechanism obtained through hydro-mechanical coupling in DEM, showing block displacement magnitudes and velocity vectors at failure.

In accordance with the yield design framework presented by Salençon (1990), it was then necessary to quantify both the work of external forces and the maximum resisting work, taking into account the self-weight of the soil and the wall, as well as the hydraulic gradient developing within regions influenced by failure mechanisms. Estimating the hydraulic component is particularly critical yet analytically difficult, and was therefore addressed through finite element modeling of hydraulic processes, performed using the CESAR-LCPC code. To support and validate the analytical developments, an experimental campaign was designed and implemented. The objective of this study is to determine the critical hydraulic height H_w that induces failure of the retaining wall, and to identify the realistic failure mechanisms involved.

3 EXPERIMENTS

3.1 *Experimental setup*

The studied problem involves creating a controlled hydraulic gradient that applies loading to both the soil and the retaining wall. In this context, an experimental campaign was conducted on 26 retaining walls, ranging in height from 17 to 40 cm, subjected to hydraulic loading up to failure. The following assumptions were adopted:

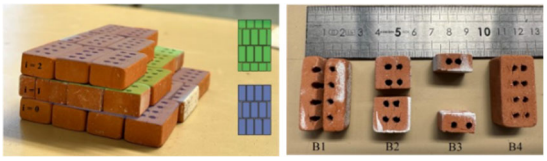

Figure 2. Bonding pattern of the experimental reduced-scale wall with crossed joints in two spatial directions, leaving the bed joints open. Fired clay bricks. B1: corner bricks, B2: half bricks, B3. quarter bricks, B4: full brick

- Saturated soil (Hostun sand HN31)
- Plane strain conditions
- Darcy-type flow
- Steady-state regime

The walls were built using fired clay bricks measuring 35.0 × 18.5 × 11.5 mm, with an average weight of 9.38 g and a material density of 16.15 kg/m³., arranged dry-stacked in a staggered bond (Fig. 2). The backfill consists of Hostun HN31 sand. A filtering geosynthetic (with an apparent opening size $O90 \approx 100$ µm) was placed at the interface between the wall and the soil to prevent the migration of sand particles through the joints of the wall. The wall–backfill assembly was installed in an acrylic glass tank with dimensions of 200 × 60 × 50 cm. These dimensions were determined based on several 3D FEM models designed to minimize boundary effects (Fig.3).

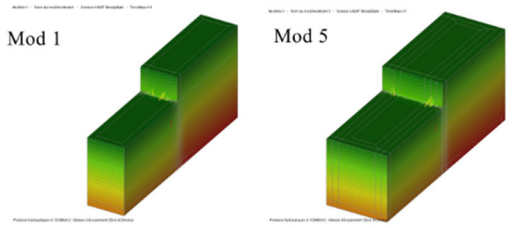

Figure 3: Example of a 3D FEM model developed for selecting the box dimensions

Furthermore, the backfilling with graded HN31 sand was carried out in successive layers, with careful attention to achieving uniform density throughout the backfill.

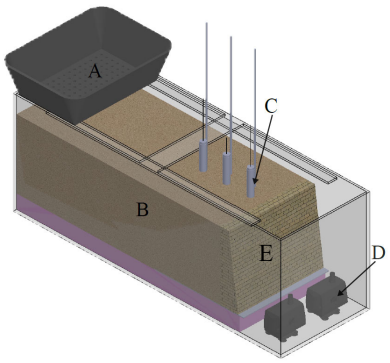

Figure 4: 3D model of the experiment (A: rainfall reservoir, B: piezometer, C: Hostun sand HN31, D: pump, E: masonry wall).

3.2 *Instrumentation and monitoring*

The experimental setup (Fig.6) was equipped with a combination of high-speed cameras and standard camcorders to monitor the behavior of both the wall and the backfill under hydraulic loading (Fig.4). Two high-speed cameras were positioned laterally to track block displacements and capture potential failure modes in real time. Depending on the wall geometry and the anticipated failure mechanism, the high-speed cameras recorded at frame rates ranging from 60 to 125 fps, while maintaining a consistent image resolution of 1024 × 2014

pixels across all tests. These recordings were complemented by two camcorders (30 fps) placed in similar positions, which proved particularly useful for observing slow movements and qualitatively capturing deformations in both the wall and the soil.These were complemented by two camcorders (30 fps) placed in similar positions, which were particularly useful for monitoring slow movements and capturing qualitative deformations in the wall and soil.

Photogrammetric targets were placed at selected points on the wall to enable precise displacement tracking. In addition, a floating marker in the downstream submerged zone was used to monitor the water level throughout the test. Synchronization between wall movements and water level changes helped in analyzing admissible flow curves and failure mechanisms.

A reference test (Test 22 with a height of 35.20 cm and a width of 7.70 cm) was also conducted using an enhanced instrumentation system. Two high-resolution cameras (5 MP, ~0.17 mm/pixel) were added near the lateral observation planes, and a stereo vision setup was implemented frontally using two 12 MP cameras (~0.16 mm/pixel). A total of 1030 images (over 103 seconds) was selected for pre-failure analysis. An additional overhead camera monitored the free surface of the water and its interaction with wall stability. For Digital Image Correlation (DIC), the outer surface of the bricks was painted white and speckled with black hydrophobic resin using an airbrush. The speckle pattern had an average diameter of 0.5 mm (about 5 pixels), with a minimum density of one spot every 4 × 4 mm.

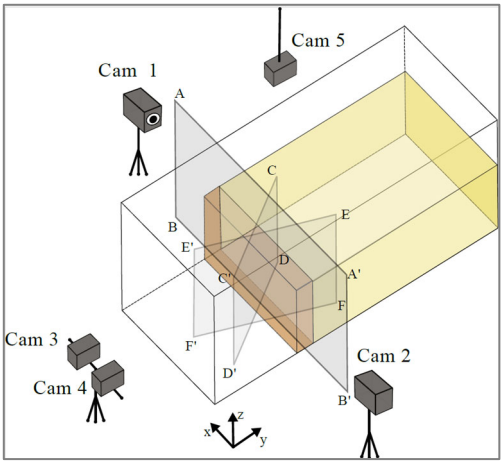

Figure 5. Instrumentation layout of the various tests conducted

4 RESULTS AND DISCUSSION

For clarity and convenience, the presentation of the experimental results will focus exclusively on the reference test, selected for its detailed instrumentation and its representativeness within the test series. As previously described, this test was monitored using a combination of techniques, including Digital Image Correlation (DIC) and optical tracking methods (referred to here as Tracker analysis), enabling a comprehensive characterization of the wall's behavior under hydraulic loading. The comparison between the experimental observations and the analytical predictions based on yield design theory will be the subject of forthcoming publications.

The Tracker analysis was performed on both lateral faces of the model, allowing the identification of the trajectories of several key blocks. Given the relatively large size and stiffness of the bricks, the displacement of each block can be reasonably approximated by the motion of its center. As a result, the displacement trajectories of points A, B, D, and D representative of different positions within the wall, were successfully extracted. This information offers valuable insights into the kinematics of the failure process, such as block rotation, translation, and interaction between units. In parallel, point W corresponding to a floating marker positioned in the downstream water basin, provided a precise and continuous measurement of the water level rise over time. By synchronizing the displacement data with the evolution of the water height Hw it was possible to track the horizontal (Ux) and vertical (Uy) displacements of the wall as a function of the hydraulic loading (Fi.g 7).

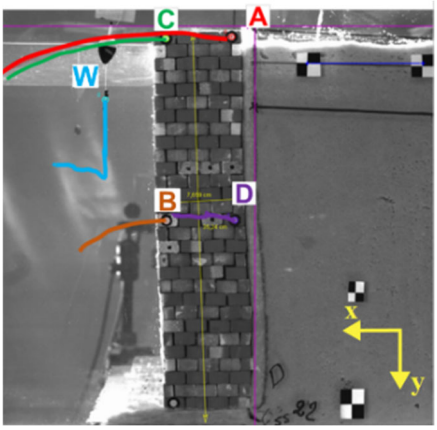

Figure 6. Illustration of the trajectories of blocks A, B, C, and D, and of the water level at point W

The resulting displacement curves clearly exhibit a nonlinear evolution, indicative of a transition from elastic deformation to plastic flow within the masonry. This transition is marked by a sudden change in the slope of the displacement curves and, in some cases, a rapid acceleration of wall movement was observed, particularly at point D, where the estimated horizontal displacement reached approximately 9.2 cm. The position of the floating marker (point W), used as a reference to track the water level, is initially located at approximately 6.8 cm from the wall head. Structural failure of the wall is observed when the water level, as indicated by the position of the float, reaches approximately 13.9 cm. This corresponds to a critical hydraulic increment H_{wc} of 7.1 cm. Given the total wall height of 35.2 cm, this critical increment represents approximately 20% of the wall height. This threshold defines the hydraulic condition under which the wall is no longer able to maintain its stability.

Furthermore, the 2D and stereo Digital Image Correlation (DIC) analyses enabled the verification of the results obtained from the Tracker-based analysis. The comparison carried out for the reference test confirmed the consistency of the measurements and also revealed the 3D effects initially predicted through finite element modeling.

Figure 7 shows the time evolution of the displacements obtained from the stereo setup (CAM3 and CAM4). The results indicate that the displacements are partially constrained along the edges, a phenomenon attributed to friction between the glass and the side walls. This effect was mitigated following recommendations from dam model testing practices (Dodaro et al. 2024), notably through the application of a lubricant (paraffin spray). Quantitatively, the maximum displacement discrepancy between two points along the same profile was estimated at 12%, a value considered non-critical and supporting the assumption of plane strain deformation for the system.

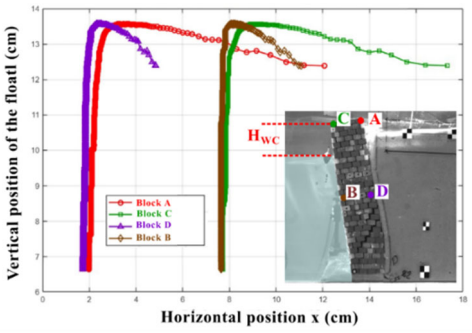

Figure 7: Variation of the horizontal position as a function of the water level (in cm) for 4 bricks of the wall

In parallel, the combined exploitation of stereo and 2D DIC data confirms the nature of the failure mechanism observed in this reference test, namely the overturning of the wall. This is further supported by the horizontal displacement field (U_x) captured post-failure (Fig.8), which shows maximum lateral displacements reaching approximately –5.2 mm in the top part of the wall. In contrast, the lower **re**gion remains near 0 mm, indicating a rotation of the structure about its base. The progressive gradient in displacement along the height of the wall is consistent with an overturning failure mode.

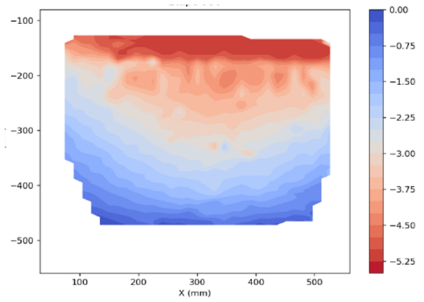

Figure 8. Post-failure horizontal displacement field Ux (in mm) obtained from stereo-DIC analysis

Across the other tests, two distinct failure mechanisms were identified: sliding, which primarily affected walls with a low slenderness ratio (less than 2), and overturning. Overall, the experimental results confirm the particular vulnerability of dry-jointed masonry retaining walls when subjected to critical hydraulic flows.

5 CONCLUSION

The comprehensive experimental investigation on masonry wall physical models under hydraulic loading provided new insights into their hydro-mechanical behavior and dominant failure mechanisms. High-resolution optical methods, including Digital Image Correlation (DIC) and Tracker-based analysis, proved effective for accurately monitoring wall displacements and capturing the onset of failure. The synchronization of wall kinematics with water level variations enabled the identification of critical hydraulic thresholds marking the transition to failure. Quantitative analysis of the displacement trajectories revealed that, near the failure threshold, point D experienced an estimated horizontal displacement of approximately 9.2 cm, while points A and C exhibited displacements of about 9.5 cm, and point B around 8.0 cm. These measurements are consistent with the displacement fields derived from 2D and stereo DIC, which provided additional spatial resolution and confirmed the presence of boundary effects. The horizontal displacement field Ux obtained post-failure displayed a maximum amplitude of −5.2−5.2 mm in the lower part of the wall, gradually decreasing toward the top—characteristic of a global overturning mechanism. Stereo DIC also validated the assumption of plane strain conditions, with edge effects within 12% of the central displacement values. These results confirm that overturning is the dominant failure mode under the tested hydraulic conditions. The study underscores the importance of multimodal instrumentation and high-resolution monitoring to fully capture the complex hydro-mechanical interactions in dry-jointed masonry structures. A detailed analytical comparison based on yield design theory is currently underway and will be presented in forthcoming work.

6 ACKNOWLEDGEMENTS

The authors would like to thank the technical staff of the RRO and Navier laboratories — especially L. Fallourd, C. Pruvost, and N. Vermorel (RRO), as well as J. Archez and G. Cumunel (Navier) — for their support during the experimental campaign. Their expertise and availability were essential to the setup and execution of the tests. Financial support from the French national research project DOLMEN is also gratefully acknowledged.

7 REFERENCES

Cerema. (2020). Analyse des risques appliquée aux murs en maçonnerie. Bron: Cerema. Collection: Références. ISBN 978-2-37180-454-8.

Colas, A. S., Morel, J. C., & Garnier, D. (2008). Yield design of dry-stone masonry retaining structures—Comparisons with analytical, numerical, and experimental data. International journal for numerical and analytical methods in geomechanics, 32(14), 1817-1832.

De Buhan, P., and de Felice, G. 1996. A homogenization approach to the ultimate strength of brick masonry. Journal of the Mechanics and Physics of Solids, 45(7), 1085–1104.

Dodaro, E., Marcolongo, M., Gottardi, G., Gragnano, C.G., Bassi, A., Stanier, S.A., and Viggiani, G.M.B. 2024. Centrifuge modelling of a river embankment slope failure induced by a high-water event. Proceedings of the 5th European Conference on Physical Modelling in Geotechnics (ECPMG 2024), Delft, the Netherlands.

Garnier, D., and Baraké, M. 2005. Analyse par la théorie du calcul à la rupture d'ouvrages de géotechnique soumis à des forces d'écoulement. Actes du 17ème Congrès Français de Mécanique.

IPCC. 2022. Climate Change 2022: Impacts, Adaptation and Vulnerability. Contribution of Working Group II to the Sixth Assessment Report of the Intergovernmental Panel on Climate Change.

Kandalai, S., John, N.J., and Patel, A. 2023. Effects of climate change on geotechnical infrastructures — state of the art. Environmental Science and Pollution Research, 30, 16878–16904.

Le, H.H. 2013. Stabilité des murs de soutènement routiers en pierre sèche : Modélisation 3D par le calcul à la rupture et expérimentation échelle 1.

Ministère de la Transition Écologique et de la Cohésion des Territoires. 2024. Plan national d'adaptation au changement climatique 3.

Phoon, K.-K. 2023. What geotechnical engineers want to know about reliability. American Society of Civil Engineers. https://doi.org/10.1061/978078448

Salençon, J. (1990). Introduction to the yield design theory and its applications to soil mechanics. European Journal of Mechanics, A/Solids, 9(5), 477-500.

Sarhosis, V., Bagi, K., Lemos, J.V., and Milani, G. 2016. Computational modeling of masonry structures using the discrete element method.

Savalle, N. 2019. Étude du comportement sismique des murs de soutènement de talus en pierre sèche.

Terrade, B., Colas, A. S., & Garnier, D. (2018). Upper bound limit analysis of masonry retaining walls using PIV velocity fields. Meccanica, 53(7), 1661-1672..